ACS APPLIED MATERIALS & INTERFACES

Research Article

www.acsami.org

Study of Band Structure at the Zn(S,O,OH)/Cu(In,Ga)Se_2 Interface via Rapid Thermal Annealing and Their Effect on the Photovoltaic Properties

Dong Hyeop Shin,[†] Seung Tae Kim,[†] Ji Hye Kim,[†] Hee Jae Kang,[‡] Byung Tae Ahn,*[,†] and HyukSang Kwon*[,†]

[†]Department of Materials Science and Engineering, Korea Advanced Institute of Science and Technology, 291 Daehak ro, Yuseong gu, Daejeon, Republic of Korea 305-701

[‡]Department of Physics, Chungbuk National University, Naesudong ro, Heung gu, Cheongju, Republic of Korea 361-763

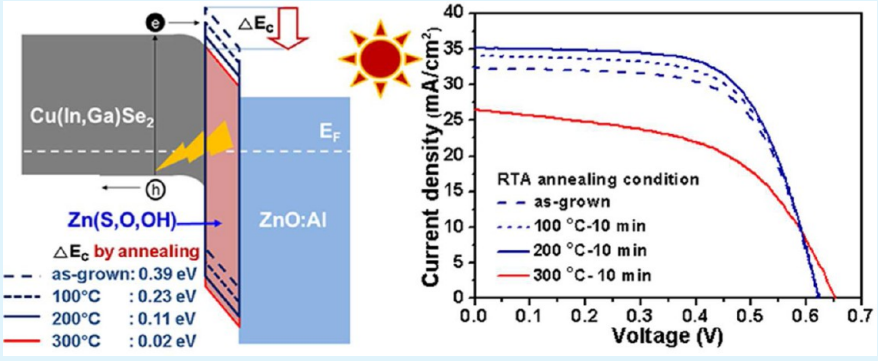

ABSTRACT: This study focused on understanding the mechanisms of the photovoltaic property changes in Zn(S,O,OH)/Cu(In,Ga)Se_2 solar cells, which were fabricated via annealing, using reflection electron energy loss spectroscopy (REELS), ultraviolet photoelectron spectroscopy (UPS), low temperature photoluminescence (LTPL), and secondary ion mass spectroscopy (SIMS). A pinhole-free Zn(S,O,OH) buffer layer was grown on a CIGS absorber layer using the chemical bath deposition (CBD). When the Zn(S,O,OH) film was annealed until 200 °C, the Zn−OH bonds in the film decreased. The band gap value of the annealed film decreased and the valence band offset (VBO) value at the Zn(S,O,OH)/CIGS interface with the annealed film increased. Both results contribute to the conduction band offset (CBO) value at the Zn(S,O,OH)/CIGS interface and, in turn, yield a reduction in the energy barrier at the interface. As a result of the annealing, the short circuit current (J_{SC}) and quantum efficiency (QE) values (400−600 nm) of the cell increased due to the improvement in the electron injection efficiency. However, when the Zn(S,O,OH) film was annealed at 300 °C, the cell efficiency declined sharply due to the QE loss in the long wavelength region (800−1100 nm). The SIMS analysis demonstrated that the Cu content in the CIGS bulk decreased and the Cu element also diffused into CIGS/Mo interface. Through LTPL analysis, it was seen that the considerable drop of the Cu content in the CIGS bulk induced a 1.15 eV PL peak, which was associated with the transition from a deep donor defect to degrade the quality of the CIGS bulk. Accordingly, the series resistance (R_S) and efficiency of the cell increased.

KEYWORDS: *Cu(In,Ga)Se_2, Zn(S,O,OH), rapid thermal annealing, conduction band offset*

1. INTRODUCTION

Cu(In,Ga)Se_2 (CIGS) thin film solar cells exhibit more than 20% efficiency, and the typical structure of high efficiency CIGS solar cells is ZnO:Al/ZnO/CdS/CIGS/Mo.[1,2] A conventional CIGS solar cell contains a CdS film as a buffer layer, and it is grown via chemical bath deposition (CBD). However, for environmental considerations, the Cd element of CdS should be removed. Moreover, the short wavelength response of CdS/CIGS solar cells is limited by the narrow band gap of CdS (≈2.42 eV). To overcome these disadvantages of CdS/CIGS solar cells, much research has focused on developing Cd-free materials for the buffer layer of CIGS solar cells such as Zn(S,O,OH) and In_2S_3.[3,4] Additionally, there are various methods to grow the Cd-free buffer layer such as CBD, atomic layer deposition, and evaporation.[3,4] At present, the Zn(S,O,OH) film grown using CBD technique is the most promising material for a Cd-free buffer layer. In laboratory scale, the Zn(S,O,OH)/CIGS solar cell has achieved up to 19.1% efficiency;[5] in commercial scale, the Zn(S,O,OH)/CIGS solar modules have realized up to 15% efficiency.[6] Nevertheless, the Zn(S,O,OH)/CIGS solar cells continue to have lower efficiency than the CdS/CIGS solar cells. In addition, only a

Received: August 22, 2013
Accepted: October 31, 2013
Published: October 31, 2013

few research groups have demonstrated high efficiency of the Zn(S,O,OH)/CIGS solar cells.[5−8]

There are various factors that make it difficult to create Zn(S,O,OH)/CIGS solar cells with efficiency levels that match those of CdS/CIGS solar cells. First, the film quality of Zn(S,O,OH) is poor due to the high solubility product of $Zn(OH)_2$ in the solution for the CBD process. The formation of $Zn(OH)_2$ creates pinholes in the film. In a previous study, a reliable process for growing defect-free Zn(S,O,OH) buffer layers on CIGS absorber layers was established.[9]

Another factor to consider in the fabrication of high efficiency CIGS solar cells is the large conduction band offset (CBO) at the Zn(S,O,OH)/CIGS interface that results from the wide band gap of the Zn(S,O,OH) buffer. The large CBO at the interface functions as an energy barrier for the electron charge carrier transport across the interface. Thus, it is very important to control the CBO of the Zn(S,O,OH)/CIGS interface in order to obtain the desirable photovoltaic characteristics of the p/n junction.

Note that the band alignment at the Zn(S,O,OH)/CIGS interface is strongly influenced by the band gap value of the buffer layer. To quantify the CBO at the interface, most researchers have used the optical band gap of the Zn(S,O,OH) film calculated from the transmittance and reflectance data gathered for the film grown on ITO or glass substrates.[10,11] However, the morphology of the film grown by the CBD process is significantly dependent on the surface condition of substrate.[12] The reported band gap values of the Zn(S,O,OH) film have varied from 3.8 to 4.0 eV, which are larger than the 3.7 eV value for pure ZnS film.[10,11] The CBO value for the 15% efficient Zn(S,O,OH)/CIGS solar cells exceeded 1.0 eV.[13] However, the reported conduction band discontinuity was too large to explain the high efficiency of the CIGS solar cells. This indicates that the uncertainty in the quantification of the CBO at the Zn(S,O,OH)/CIGS interface partially originated from the incorrect determination of the band gap value of the Zn(S,O,OH) film grown on the ITO or glass substrates. To date, detailed reports have not been available on the direct band gap measurement of Zn(S,O,OH) film grown on the CIGS film.

To obtain a desirable Zn(S,O,OH)/CIGS interface for high efficiency solar cells, the analysis of the band alignment at the interface should be conducted accurately. For this purpose, the band gap value of the Zn(S,O,OH) film grown on the CIGS film was measured by reflection electron energy loss spectroscopy (REELS), which is a well-known tool for the measurement of band gap value for wide band gap semiconductor or dielectric materials.[14,15] The valence band offset (VBO) value at the Zn(S,O,OH)/CIGS interface was analyzed using ultraviolet photoelectron spectroscopy (UPS) with an Ar ion etching gun. A rapid thermal annealing (RTA) process has several advantages such as a lower thermal budget and precise processing time compared with furnace annealing. Thus, the RTA process was used to minimize the interdiffusion of the interface. The CBO at the interface was modified via RTA process. The effect of the RTA process on the performance of the Zn(S,O,OH)/CIGS solar cells was investigated, and the RTA process was optimized to achieve high efficiency Zn(S,O,OH)/CIGS solar cells.

2. EXPERIMENTAL SECTION

2.1. Thin Film Growth and Device Fabrication. To investigate the effect of post annealing on the performance of Zn(S,O,OH)/CIGS solar cells, the CIGS absorber layers were deposited on Mo-coated glass substrates by a three stage process. A detailed description of the CIGS film deposition procedure can be found in the earlier work.[16,17] The CIGS film composition was adjusted as $Cu(In_{0.7}Ga_{0.3})Se_2$ using energy dispersive X-ray spectroscopy. The Zn(S,O,OH) buffer layers were grown on the CIGS absorber layers using the CBD process from an aqueous solution of zinc sulfate ($ZnSO_4{\cdot}7H_2O$; 99.99% purity Sigma-Aldrich), thiourea ($(NH_2)_2CS$; 99.0% purity, Sigma-Aldrich), and ammonia hydroxide (NH_4OH; 28% purity, Sigma-Aldrich).[9] When the concentrations of $ZnSO_4$, $(NH_2)_2CS$, and NH_4OH in the solution were 0.1, 0.6, and 7.0 M, respectively, pinhole-free Zn(S,O,OH) buffer layers were grown on the CIGS absorber layers. After the Zn(S,O,OH) buffer growth was completed, the sample was washed sequentially with 0.5 M ammonia solution and deionized water.[18] A detailed description of the Zn(S,O,OH) film growth procedure can be found in the earlier work.[9] The samples were annealed in ambient air using a RTA process. With the advantages of a lower thermal budget and precise processing time, the RTA process was used to minimize the interdiffusion of the Zn(S,O,OH)/CIGS interface. To investigate the effect of the annealing temperature on the cell performance, the annealing temperature was varied from 100 to 300 °C with the annealing time fixed at 10 min. Then, the samples were left to cool naturally.

To fabricate Zn(S,O,OH)/CIGS solar cells, a ZnO:Al film with a bilayer structure was deposited on the Zn(S,O,OH) buffer layer using RF magnetron sputtering.[19] Finally, the Al grid was deposited using a thermal evaporator.

2.2. Film and Device Characterization. The morphology and thickness of the Zn(S,O,OH) films were verified via scanning electron microscopy (SEM); FEI Nova 230. The chemical composition of the Zn(S,O,OH) film was verified via X-ray photoelectron spectroscopy (XPS); Thermo Fisher VG Scientific Sigma Probe. To determine the VBO value at the Zn(S,O,OH)/CIGS interface, the valence band maximum (VBM) value was measured via UPS; Thermo Fisher VG Scientific Sigma Probe. The VBO value at the interface was obtained via etching the film in the soft conditions of an Ar ion etching gun intensity (1 kV, 1 μA) to minimize film damage.[20] To calculate the CBO at the interface, the band gap value of the Zn(S,O,OH) film was obtained from the REELS; VG ESCALAB 210. The REELS spectrum was measured with primary electron energy of 1.5 keV for the excitation.[12,14] The depth profile of each element in the CIGS film was verified via secondary ion mass spectroscopy (SIMS) measurement using Cs^+ ion as the primary ion. The photoluminescence (PL) spectrum of the CIGS film was measured at 10 K using a He−Ne ion laser with an excitation wavelength of 633 nm and an LN2 cooled CCD detector.

The current density−voltage (J−V) characteristics of the solar cells were measured under one sun condition with 1.5 AM using an Oriel Solar Simulator 300 W.[9] The spectral quantum efficiency (QE) spectrum was measured using a PV Measurement QEX7.[9]

3. RESULTS AND DISCUSSION

Figure 1 shows the surface (a, c) and cross section (b, d) SEM images of the Zn(S,O,OH) films grown on the CIGS and ITO films. A CBD process for 20 min yielded an approximately 30 nm thick Zn(S,O,OH) film. The film completely covered the CIGS surface and did not have pinholes. The film morphology revealed a fine grain structure and the grain sizes varied in the range of 5 to 10 nm. The film perfectly covered the grain boundaries of the CIGS film (Figure 1a). However, when the Zn(S,O,OH) film was grown on the ITO substrate, the film did not perfectly cover the ITO film due to the substrate effect. The underlying surface of the ITO film is clearly visible in Figure 1c. In addition, the surface morphology of the film grown on the ITO substrate exhibited a hemispheric shape that might be induced by the different surface energies of the substrate.[12] Considering the imperfect coverage of the Zn(S,O,OH) film on the ITO film, it was difficult to estimate the optical band gap of

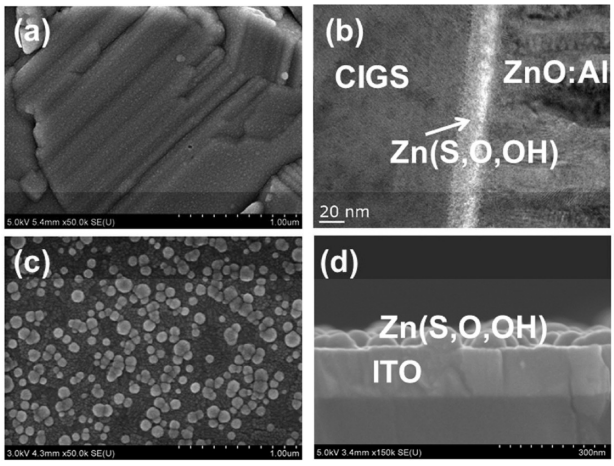

Figure 1. Surface (a, c) and cross-sectional (b, d) SEM images of the Zn(S,O,OH) films grown on the CIGS and ITO films.

the Zn(S,O,OH) film on the CIGS film through transmittance-reflectance measurements of the Zn(S,O,OH) film on the ITO film.

Figure 2 presents the $J-V$ (a) and QE curves (b) of the CIGS solar cells fabricated with the as-grown Zn(S,O,OH) and annealed Zn(S,O,OH) buffers with temperatures varying from 100 to 300 °C for 10 min. The annealing of the Zn(S,O,OH) buffer layer in the temperature range from 100 to 200 °C resulted in a significant improvement of the $J-V$ characteristics. The photovoltaic parameters of the cells are summarized in Table 1. As the annealing temperature increased to 200 °C, the short circuit current (J_{SC}) increased from 32.3 to 35.1 mA/cm^2 and the cell efficiency was improved from 13.04 to 14.22%. In contrast, the CIGS solar cell with the 300 °C annealed buffer exhibited poor $J-V$ characteristics. Although the cells have showed similar values in the open circuit voltage, the J_{SC} and FF were significantly decreased. Thus, the cell performance decreased sharply to 9.2%. With annealing up to 200 °C, the QE curves showed that the spectral response in the short wavelength region increased (Figure 2b). The considerable rise in the QE values of the solar cell with the 200 °C annealed buffer suggests that the carrier transport across the Zn-(S,O,OH)/CIGS interface was enhanced and the band alignment at the interface was more favorable. At 300 °C annealing, the spectral response decreased both in the short wavelength region and long wavelength region. The decrease of the QE value in the short wavelength region was due to lower band gap of the Zn(S,O,OH) film as described in Figure 4. Note that the QE values of the long wavelength region were sharply decreased. Thus, the QE spectrum for the CIGS solar cell with the 300 °C annealed buffer was measured under −1 V reverse bias. The QE ratio with −1 V reverse bias and zero bias is seen in Figure 2c. The QE(−1 V)/QE(0 V) ratio in the long wavelength region (800−1100 nm) was increased, while the QE(−1 V)/QE(0 V) ratio in the short wavelength region (300−600 nm) was flat. The lower QE value and increase of the QE(−1 V)/QE(0 V) ratio at the long wavelength suggest the degradation of the CIGS bulk. The origin of this degradation is discussed later.

To investigate the chemical state of the Zn(S,O,OH)/CIGS interface, the XPS depth profile of the interface was verified via etching the films with an Ar ion gun. Figure 3 shows the XPS depth profiles of the constituent elements at the Zn(S,O,OH)/

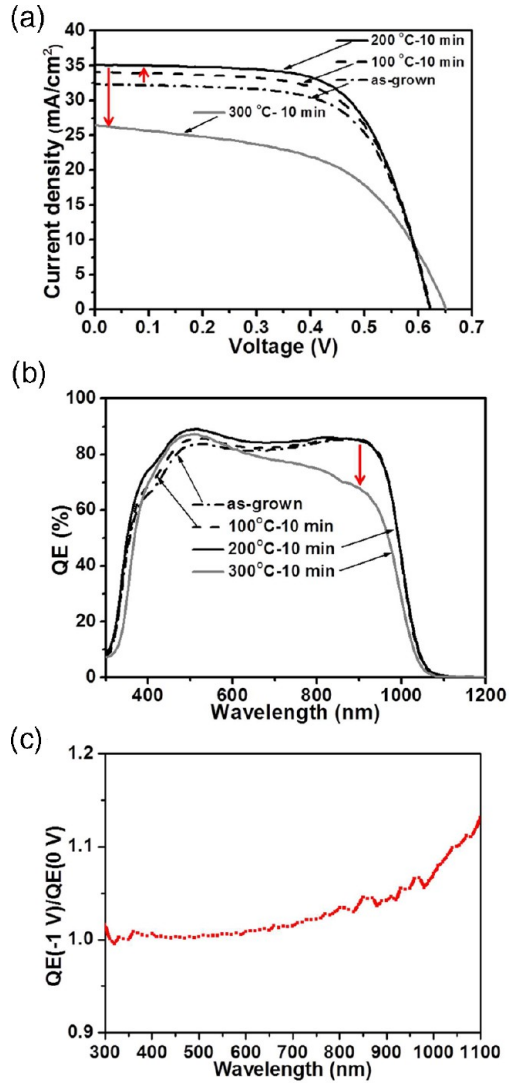

Figure 2. (a) $J-V$ and (b) QE curves of CIGS solar cells fabricated with the as-grown Zn(S,O,OH) and annealed Zn(S,O,OH) buffers at the temperatures varied from 100 to 300 °C for 10 min. (c) QE(−1 V) /QE(0 V) ratio of CIGS solar cell fabricated with the annealed Zn(S,O,OH) buffer at 300 °C for 10 min.

Table 1. Photovoltaic Parameters of CIGS Solar Cells Fabricated with the as-grown Zn(S,O,OH) and Annealed Zn(S,O,OH) Buffers at Temperatures Varied from 100 to 300 °C

temp.	V_{OC}	J_{SC}	FF	η	R_S	R_{Sh}
as-grown	0.62	32.30	65.03	13.04	1.19	551.9
100 °C	0.62	34.06	64.21	13.64	1.15	576.4
200 °C	0.62	35.10	65.10	14.22	1.10	807.5
300 °C	0.65	26.45	53.38	9.20	2.17	205.1

CIGS interfaces with the as-grown Zn(S,O,OH) and annealed Zn(S,O,OH) buffers at temperatures varied from 100 to 300 °C. After annealing via the RTA process, a significant interdiffusion of each element at the interface was not observed. The chemical state of the as-grown film is characterized as follows: 65% Zn−S, 12% Zn−O, and 23% Zn−OH bonds. The Zn−OH bonds originated from the reaction of hydroxide ions with Zn complex ions in the basic solution. When the sample was annealed at 100 to 200 °C, the Zn−OH bonds in the film

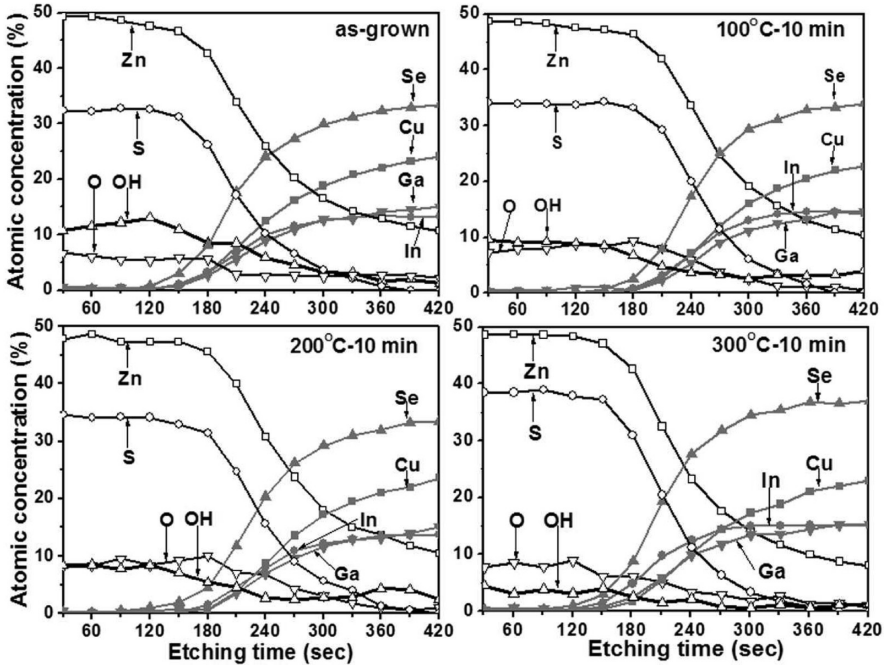

Figure 3. XPS depth profiles of the constituent elements at the Zn(S,O,OH)/CIGS interfaces with the as-grown Zn(S,O,OH) and annealed Zn(S,O,OH) buffers at temperatures varied from 100 to 300 °C.

decreased significantly. After annealing at 300 °C, the concentration of Zn−OH bonds was further reduced from 23 to 9%. The Zn−OH bonds could be dehydrated under 200 °C with the following reaction: 2(Zn−OH) → (Zn−O) + H_2O, due to low decomposition temperature of $Zn(OH)_2$ (125 °C).[21] This indicates that many Zn−OH bonds were converted to Zn−O bonds via the annealing process. Thus, as the annealing temperature increased, the concentration of the Zn−OH bonds decreased and the [Zn−O]/([Zn−O] + [Zn−OH]) ratio increased. At 300 °C annealing, 5% Zn−O bonds were gained at the expense of Zn−OH by dehydration. It can be expected that the reduction of the Zn−OH bonds affects the band structure and, in turn, the properties of the pn junction. It is known that the existence of the Zn−OH bond in the film negatively influences on the quality of the p/n junction in the CIGS solar cells. Some literatures reported that the Zn−OH bond induces stability issues of Zn(S,O,OH)/CIGS solar cells.[9,21] In this regard, it is crucial to reduce the content of Zn−OH bonds in the film for high efficiency CIGS solar cells.

To investigate the band structure at the Zn(S,O,OH)/CIGS interface, the band gap value of Zn(S,O,OH) film grown on the CIGS film was measured directly using REELS and the valence-band binding energies of the Zn(S,O,OH) film were measured using UPS. The combination of REELS and UPS analyses enabled the determination of the conduction band offset (CBO) at the interface with the following relation:

$$\mathrm{CBO}_{\mathrm{Zn(S,O,OH)/CIGS}} = E_g^{\mathrm{Zn(S,O,OH)}} - E_g^{\mathrm{CIGS}} - \mathrm{VBO}_{\mathrm{Zn(S,O,OH)/CIGS}}$$

Generally, the band gap values of the Zn(S,O,OH) film could be determined using the transmittance−reflectance measurements with a UV−visible spectrometer. However, in this case, the aforementioned method is not suitable due to the substrate effect (Figure 1). Therefore, reflection electron energy loss spectroscopy (REELS) was used to directly measure the band gap values of the Zn(S,O,OH) film on the CIGS film.

Figure 4 shows the REELS spectra of the as-grown Zn(S,O,OH) and annealed Zn(S,O,OH) films at temperatures varied from 100 to 300 °C. The band gap value was determined from the electron energy loss spectrum.[12,14] The band gaps of the as-grown film and annealed films at 100 to 300 °C were 3.42, 3.34, 3.32, and 3.27 eV, respectively. As the annealing temperature increased, the band gap values of the annealed films gradually decreased. This tendency is in agreement with the decreasing Zn−OH bonds in the XPS data, as shown in Figure 3. It is known that band gap value of Zn(S,O,OH) compound film shows bowing curve depending on the ratio of oxygen.[22,23]

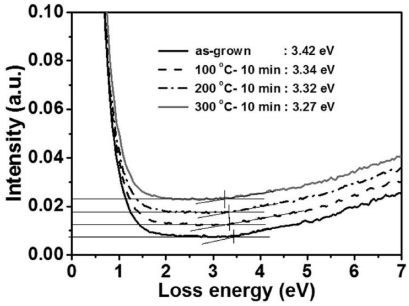

Figure 4. REELS spectra of the as-grown Zn(S,O,OH) and annealed Zn(S,O,OH) films at temperatures varied from 100 to 300 °C.

The UPS depth analyses were used to assess the electronic structure of the interface. The UPS spectrum provides the VBM position of the Zn(S,O,OH) and CIGS films. The valence band discontinuity was acquired from the VBM position changes of the Zn(S,O,OH) and CIGS films through etching the film. Figure 5 shows the UPS spectra at the Zn(S,O,OH)/CIGS interface with the as-grown Zn(S,O,OH) and annealed

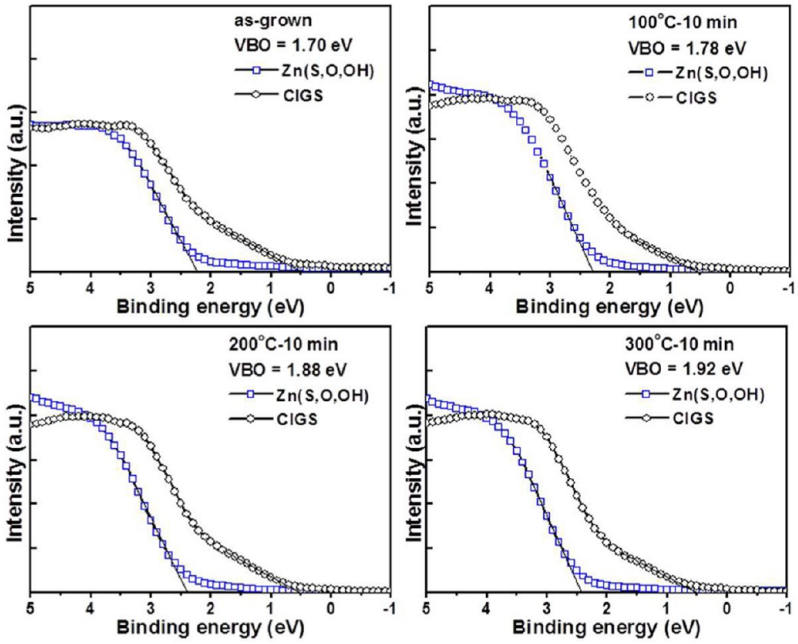

Figure 5. UPS spectra at the Zn(S,O,OH)/CIGS interface with the as-grown Zn(S,O,OH) and annealed Zn(S,O,OH) films at temperatures varied from 100 to 300 °C.

Zn(S,O,OH) films at temperatures varied from 100 to 300 °C. The binding energy scale is referred to the Fermi level. It was found that the VBM value was 0.5 eV for the CIGS films and this value is independent of the annealing temperature. The VBM values of the as-grown Zn(S,O,OH) film and annealed Zn(S,O,OH) films at 100 to 300 °C were 2.20, 2.28, 2.38, and 2.42 eV, respectively. Therefore, the VBO values of the as-grown film and annealed films at 100 to 300 °C were 1.70, 1.78, 1.88, and 1.92 eV, respectively. Considering the XPS depth profiles in Figure 3, the change in the VBO value at the interface was clearly related to the reduction of the Zn−OH bonds in the film upon annealing. It was found that the annealing process modified the valence band discontinuity at the Zn(S,O,OH)/CIGS interface as well as the band gap value of the Zn(S,O,OH) film.

Figure 6 shows the calculated CBO values at the Zn(S,O,OH)/CIGS interface according to the annealing temperatures varied from 100 to 300 °C. The band gap of the CIGS surface can be calculated from the relation of from the relation of $E_g = 1.018 + 0.575X + 0.108X^2$ where is $X = [Ga]/([In] + [Ga])$.[24] The composition of CIGS surface was estimated as $Cu(In_{0.5}Ga_{0.5})Se_{2-\delta}$ by XPS analysis (Figure 3). Thus, the band gap of CIGS surface was calculated as 1.33 eV. Some literatures reported the existence of ordered vacancy compound phase with 1.34 eV at the CIGS surface.[25−27] In that case, 1.34 eV for band gap of CIGS surface might be applied. To calculate the CBO value at the Zn(S,O,OH)/CIGS interface, 1.33 eV was used for the band gap value of the CIGS surface. As the annealing temperature increased, the CBO values at the interface gradually decreased from 0.39 to 0.02 eV. The schematic of the p/n junction in the figure exhibits the change of the energy band diagram upon annealing. After annealing via the RTA process, the CBO value at the interface decreases due to increase of VBO value and reduction in the band gap of Zn(S,O,OH) film. In general, the CBO value corresponds to the energy barrier height at the interface. Thus, the annealing process reduced the energy barrier at the interface and, in turn, increased the J_{SC} and QE values of the cells until 200 °C through improving the electron injection efficiency at the interface (Figure 2). The obtained results demonstrate that the annealing process can be used to tailor the conduction band alignment at the interface in order to increase the efficiency of the CIGS solar cells. This suggestion is in agreement with the photovoltaic parameter changes upon annealing. Recent literatures reported that the CBO value at the interface could be affect by heat and light soaking process.[28,29]

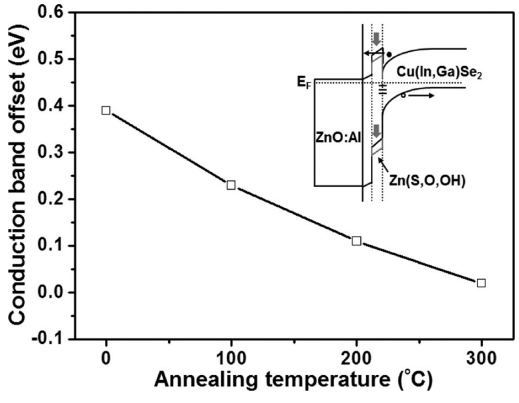

Figure 6. Calculated CBO values at the Zn(S,O,OH)/CIGS interface according to annealing temperatures varied from 100 to 300 °C.

Although the annealing process has a positive effect on the Zn(S,O,OH)/CIGS solar cell, the 300 °C annealing degraded the cell performance by decreasing the QE values in the long wavelength region (Figure 2b). Generally, the spectral response in the long wavelength region is closely related to the CIGS film quality. It is known that the Cu content in the CIGS film influences on the electrical properties.[30] To estimate the Cu content in the CIGS film, SIMS depth profiling was conducted.

Figure 7 shows the SIMS profiles of the Cu content in the Zn(S,O,OH)/CIGS films according to the annealing temperatures varied from 200 to 300 °C. The surface of the CIGS film

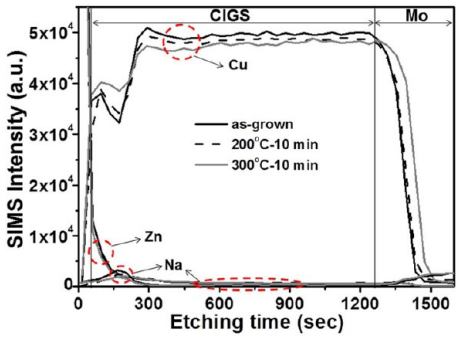

Figure 7. SIMS profiles of Cu content in the Zn(S,O,OH)/CIGS films according to annealing temperatures varied from 200 to 300 °C.

showed more Cu-deficient region compared with the CIGS bulk. At 200 °C annealing, the Cu content of the CIGS bulk decreased slightly. However, after annealing at 300 °C, the Cu content of the CIGS surface increased and the Cu element was noticeably diffused into the CIGS/Mo interface. Furthermore, a considerable drop was observed in the Cu content of the CIGS bulk region. However, regardless of annealing process, the Na content of the CIGS bulk was constant and Zn element was not significantly diffused into the CIGS surface.

To understand the negative effect of the Cu content reduction in the CIGS film on the cell performance, a low temperature photoluminescence (LTPL) was conducted at 10 K. Figure 8 shows the LTPL spectra of the as-grown

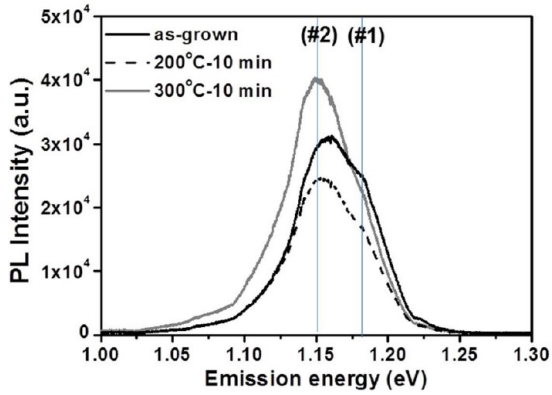

Figure 8. LTPL spectra of the as-grown Zn(S,O,OH)/CIGS and Zn(S,O,OH)/CIGS films with annealing at 200 and 300 °C.

Zn(S,O,OH)/CIGS and Zn(S,O,OH)/CIGS films with annealing at 200 and 300 °C. All Zn(S,O,OH)/CIGS films showed two peaks: 1.18 eV (#1) and 1.15 eV (#2). Peak (#1) is related to a transition between very shallow defect levels or band-defect transition. This emission is expected to be associated with the transition from a Se vacancy or band to a Cu vacancy (V_{Cu}) or other shallow acceptor.[31−33] Peak (#2) is related to a donor−acceptor pair transition. This peak may be associated with the transition from deep donor defect such as an $In_{Cu}-V_{Cu}$ complex to V_{Cu} or another shallow acceptor.[31−33] When the annealing temperature increased to 300 °C, the intensity of peak (#2) increased sharply. This indicates that the reduction of the Cu content in the CIGS film through annealing at 300 °C can form a deep donor defect and degrade the film quality. The increase in the deep level PL peak (#2) can cause a decrease in the carrier mobility and diffusion length. As a result, the series resistance (R_S) of the cell increased and the FF value of the cell decreased, as shown in Table 1.

Cd-free buffer materials for environmentally friendly CIGS solar cells have wide band gaps that can suppress charge injections from the CIGS layer to the buffer layer. RTA processes can be used to modify the junction band structure. From the aforementioned results, it is clear that the enhanced current collection at the junction without film degradation is a very important factor for high efficiency solar cells. It is believed that the experimental results and their analysis in this study will be beneficial in improving the efficiency of other Cd-free solar cells.

4. CONCLUSIONS

For environmentally friendly CIGS solar cells, a pinhole-free Zn(S,O,OH) buffer layer was grown on a CIGS absorber layer using a chemical bath deposition. To enhance the current collection at the Zn(S,O,OH)/CIGS interface, an RTA process of the interface was used. As a result, as the annealing temperature increased to 200 °C, the J_{SC} value and efficiency of the Zn(S,O,OH)/CIGS solar cells increased gradually. However, at 300 °C annealing, the cell efficiency declined sharply due to the low J_{SC} and FF, which were caused by the lowered QE values in the long wavelength region (800−1100 nm). As the annealing temperature increased, the Zn−OH bonds in the Zn(S,O,OH) film were reduced via dehydration. Through the annealing, the band gap value of the annealed Zn(S,O,OH) film decreased and the VBO value at the interface increased. Thus, the CBO value at the interface decreased. The decrease of the CBO value at the interface yielded a decrease in the energy barrier and in turn increased the J_{SC} and QE values (400−600 nm) through improving the electron injection efficiency. At 300 °C annealing, the efficiency dropped due to the Cu redistribution. The Cu content of the CIGS surface increased at the CIGS surface and the Cu element was noticeably diffused into the CIGS/Mo interface. Also, the Cu content in the CIGS bulk region decreased. According to the LTPL analysis, the considerable drop in the Cu content induced a deep level PL peak. Additionally, the R_S value of the cell increased and the FF value decreased. In conclusion, the annealing process significantly affected the band alignment of the Zn(S,O,OH)/CIGS interface and, in turn, the solar cell performance. Through optimization of the annealing process, an efficiency of 14.8% was achieved.

AUTHOR INFORMATION

Corresponding Authors

*E-mail: btahn@kaist.ac.kr.
*E-mail: hskwon@kaist.ac.kr.

Notes

The authors declare no competing financial interest.

ACKNOWLEDGMENTS

This work was supported by the Basic Science Research Program through the National Research Foundation of Korea (NRF) funded by the Ministry of Education (2009-0094038) and the Center for Inorganic Photovoltaic Materials (No. 2012-0001167) grant funded by the Korean government (Ministry of Science, ICT & Future Planning).

REFERENCES

(1) Jackson, P.; Hariskos, D.; Lotter, E.; Paetel, S.; Wuerz, R.; Menner, R.; Wischmann, W.; Powalla, M. *Prog. Photovoltaics* **2011**, *19*, 894−897.
(2) Repins, I.; Contreras, M. A.; Egaas, B.; DeHart, C.; Scharf, J.; Perkins, C. L.; To, B.; Noufi, R. *Prog. Photovoltaics* **2008**, *16*, 235−239.
(3) Hariskos, D.; Spiering, S.; Powalla, M. *Thin Solid Films* **2005**, *480−481*, 99−109.
(4) Naghavi, N.; Abou-Ras, D.; Allsop, N.; Barreau, N.; Bucheler, S.; Ennaoui, A.; Fischer, C. H.; Guillen, C.; Hariskos, D.; Herrero, J.; Klenk, R.; Kushiya, K.; Licont, D.; Menner, R.; Nakada, T.; Platzer-Bjorkman, C.; Spiering, S.; Tiwari, A. N.; Torndahl, T. *Prog. Photovoltaics* **2010**, *18*, 411−433.
(5) Hariskos, D.; Menner, R.; Jackson, P.; Paetel, S.; Witte, W.; Wischmann, W.; Powalla, M.; Burkert, L.; Kolb, T.; Oertel, M.; Dimmler, D.; Fuchs, B. *Prog. Photovoltaics* **2012**, *20*, 534−542.
(6) Kyshiya, K.; Tanaka, Y.; Hakuma, H.; Goushi, Y.; Kijima, S.; Aramoto, T.; Fujiwara, Y. *Thin Solid Films* **2009**, *517*, 2108−2110.
(7) Nakada, T.; Mizutani, M. *Jpn. J. Appl. Phys.* **2002**, *41*, L165−L167.
(8) Hubert, C.; Naghavi, N.; Roussel, O.; Etcheberry, A.; Hariskos, D.; Menner, R.; Powalla, M.; Kerrec, O.; Lincot, D. *Prog. Photovoltaics* **2009**, *17*, 470−478.
(9) Shin, D. H.; Kim, J. H.; Kim, S. T.; Larina, L.; Al-Ammar, E. A.; Ahn, B. T. *Sol. Energy Mater. Sol. Cells* **2013**, *116*, 76−82.
(10) Bar, M.; Ennaoui, A.; Klaer, J.; Saez-Araoz, R.; Kropp, T.; Weinhardt, L.; Heske, C.; Schock, H. W.; Fischer, Ch. H.; Lux-Steiner, M. C. *Chem. Phys. Lett.* **2006**, *433*, 71−74.
(11) Shin, S. W.; Kang, S. R.; Yun, J. H.; Moholkar, A. V.; Moon, J. H.; Lee, J. Y.; Kim, J. H. *Sol. Energy Mater. Sol. Cells* **2011**, *95*, 856−863.
(12) Hodes, G. Marcel Dekker: New York/Basel, 2006, 23.
(13) Nakada, T.; Hongo, M.; Hayashi, E. *Thin Solid Films* **2003**, *431−432*, 242−248.
(14) Jin, H.; Oh, S. K.; Kang, H. J.; Cho, M. H. *Appl. Phys. Lett.* **2006**, *89*, 122901−3.
(15) Tahir, D.; Lee, E. K.; Oh, S. K.; Tham, T. T.; Kang, H. J.; Jin, H.; Park, J. C.; Chung, J. G.; Lee, J. C. *Appl. Phys. Lett.* **2009**, *94*, 212902−3.
(16) Kim, K. H.; Yoon, K. H.; Yun, J. H.; Ahn, B. T. *Electrochem. Solid-State Lett.* **2006**, *9*, A382−A385.
(17) Shin, D. H.; Shin, Y. M.; Kim, J. H.; Ahn, B. T.; Yoon, K. H. *J. Electrochem. Soc.* **2012**, *159*, B1−B5.
(18) Ennaoui, A.; Bar, M.; Klaer, J.; Kropp, T.; Szez-Araoz, R.; Lux-Steiner, M. Ch. *Prog. Photovoltaics* **2006**, *14*, 499−511.
(19) Shin, D. H.; Kim, J. H.; Shin, Y. M.; Yoon, K. H.; Al-Ammar, E. A.; Ahn, B. T. *Prog. Photovoltaics* **2013**, *21*, 217−225.
(20) Larina, L.; Shin, D. H.; Kim, J. H.; Ahn, B. T. *Energy Environ. Sci.* **2011**, *4*, 3487−3493.
(21) Kushiya, K.; Yamase, O. *Jpn. J. Appl. Phys.* **2000**, *39*, 2577−2582.
(22) Persson, C. *Phys. Rev. Lett.* **2006**, *97*, 146403−4.
(23) Bar, M.; Reichardt, J.; Grimm, A.; Kostschau, I.; Lauermann, I.; Rahne, K.; Sokoll, S.; Weinhardt, L.; Umbach, E.; Heske, C.; Jung, Ch.; Niesen, T. P.; Visbeck, S. *J. Appl. Phys.* **2005**, *98*, 053702−8.
(24) Birkmire, R. W.; Eser, E. *Annu. Rev. Mater. Sci.* **1997**, *27*, 625−653.
(25) Zhang, Z.; Tang, X.; Lemmer, U.; Witte, W.; Kiowski, O.; Powalla, M.; Holscher, H. *Appl. Phys. Lett.* **2011**, *99*, 042111−3.
(26) Kemell, M.; Ritala, M.; Leskela, M. *Crit. Rev. Solid State Mater. Sci.* **2005**, *30*, 1−31.
(27) Schmid, D.; Ruckh, M.; Grunwald, F.; Schock, H. W. *J. Appl. Phys.* **1993**, *73*, 2902−2909.
(28) Kobayashi, T.; Yamaguchi, H.; Nakada, T. *Prog. Photovoltaics* **2013**, 10.1002/pip.2339.
(29) Nakada, T.; Kobayashi, T.; Kumazawa, T.; Yamaguchi, H. *IEEE J. Photovoltaics* **2013**, *3*, 461−466.
(30) Lee, D. Y.; Kim, M. S.; Larina, L.; Ahn, B. T. *Electron. Mater. Lett.* **2008**, *4*, 13−18.
(31) Shin, Y. M.; Lee, C. S.; Shin, D. H.; Ko, Y. M.; Al-Ammar, E. A.; Kwon, H. S.; Ahn, B. T. *ECS J. Solid State Sci. Technol.* **2013**, *2*, P1−P5.
(32) Zott, S.; Leo, K.; Ruckh, M.; Schock, H. W. *Appl. Phys. Lett.* **1996**, *68*, 1144−1146.
(33) Ishizuka, S.; Yamada, A.; Islam, M. M.; Shibata, H.; Fons, P.; Sakurai, T.; Akimoto, K.; Niki, S. *J. Appl. Phys.* **2009**, *106*, 034908−6.